ChemComm

Partially fluorinated polymer network enhances Li-ion transference number of sulfolane-based highly concentrated electrolytes

Journal:	*ChemComm*
Manuscript ID	CC-COM-08-2024-004291.R1
Article Type:	Communication

ChemComm

COMMUNICATION

Partially fluorinated polymer network enhances Li-ion transference number of sulfolane-based highly concentrated electrolytes

Received 00th January 20xx,
Accepted 00th January 20xx

DOI: 10.1039/x0xx00000x

Yukako Konishi,[a] Hisashi Kokubo,[a] Seiji Tsuzuki,[b] Ryoichi Tatara [a,b] and Kaoru Dokko *[a,b]

Gelation of sulfolane-based highly concentrated electrolytes using a partially fluorinated polymer enhances Li-ion transference number of the electrolytes because acidic protons surrounded by fluorine atoms in the polymer network trap anions, and the high Li^+ transference number is effective in suppressing the concentration polarization in Li batteries.

Lithium-ion batteries (LIBs) are widely used in various applications ranging from portable electronic devices to electric vehicles because of their high energy and power densities. Unlike the flammable organic liquid electrolytes widely used in LIBs, sulfolane (SL) is a thermally stable and non-flammable solvent that can dissolve large amounts of Li salts.[1,2] Highly concentrated electrolytes (HCEs) have attractive properties to promote battery applications, such as high thermal stability and a wide electrochemical window.[3–5] We have reported that Li^+ ion-hopping conduction occurs in SL-based HCEs.[6–8] The SL-based HCEs have a unique solvation structure, in which Li^+ ions are crosslinked with SL molecules and anions. These Li^+ ions can dynamically exchange their ligands (SL and anions); thus, they can diffuse and migrate faster than the ligands, resulting in a high Li-ion transference number (t_{Li+}). A high t_{Li+} value of the electrolyte is effective in suppressing concentration polarization during high-rate charging and discharging of LIBs.[6,8]

The gelation of HCEs can prevent the leakage of liquids and further improve the safety of LIBs.[9,10] In gel polymer electrolytes, liquid electrolytes are incorporated into a polymer network.[11–14] The Li^+-ion transport properties of gel electrolytes are affected by not only the parent liquid electrolyte but also the structure of the polymer network, because the solvation structure of Li^+ changes during gelation owing to the interaction between the functional groups of the polymer matrix and ion species.[15,16] Thus, the selection of an appropriate polymer structure is important for improving the performance of LIBs with gel electrolytes.

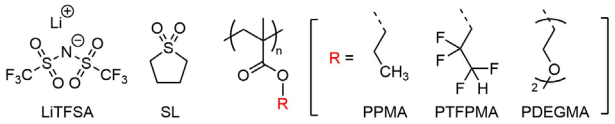

Fig. 1. Chemical structures of LiTFSA, SL, PPMA, PTFPMA, and PDEGMA.

In this study, we investigated the effect of the side chain structure of a polymer on the Li-ion transport properties of gel electrolytes. Gel electrolytes composed of an SL-based HCE and methacrylate-based polymers with different side chains were prepared (**Fig. 1**), and the interactions between the functional groups on the polymer side chain and ionic species in the gels were analyzed. The Li-ion transport properties of the gel electrolyte change depending on the functional group, because the side chain–ion interaction significantly affects the Li^+ ion solvation structure and mobility of ions. Here, we demonstrated that the interaction between a partially fluorinated side chain and an anion is effective in enhancing the t_{Li+} value of gel electrolytes, and that a high t_{Li+} of gel electrolytes promotes the mitigation of concentration polarization in LIBs during discharging.

In this study, a liquid electrolyte consisting of lithium bis(trifluoromethanesulfonyl)amide (LiTFSA) and SL mixed at a molar ratio of 1:3 was gelated using methacrylate-based polymers. The [LiTFSA]/[SL] = 1/3 solution was selected as a model liquid electrolyte because this solution is a glass forming liquid and maintains liquid state over a wide temperature range (**Fig. S1**).[7] Gel electrolytes containing the [LiTFSA]/[SL] = 1/3 solution were prepared by free radical polymerization. Three different methacrylate monomers were used for gelation: propyl methacrylate (PMA), 2,2,3,3-tetrafluoropropyl methacrylate (TFPMA), and diethylene glycol monomethyl

[a] *Department of Chemistry and Life Science, Yokohama National University, 79-5 Tokiwadai, Hodogaya-ku, Yokohama 240-8501, Japan.*
[b] *Advanced Chemical Energy Research Centre, Institute of Advanced Sciences, Yokohama National University, 79-5 Tokiwadai, Hodogaya-ku, Yokohama 240-8501, Japan.*
Supplementary Information available. See DOI: 10.1039/x0xx00000x

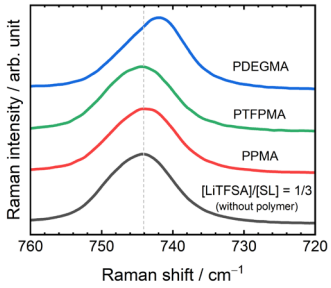

Fig. 2. Raman spectra of polymer solutions [LiTFSA]/[SL]/[monomer unit] = 1/3/1 and the [LiTFSA]/[SL] = 1/3 solution (without any polymer) at 30 °C.

ether methacrylate (DEGMA). These monomers were selected as model monomer units for the polymer network because PMA has a simple alkyl side chain, TFPMA has a partially fluorinated side chain which may interact with the fluorinated anion, and DEGMA has ether oxygens that can interact with Li^+. The chosen methacrylate monomer, a crosslinker (ethylene glycol dimethacrylate, EGDMA), and an initiator (2,2′-azobis(isobutyronitrile), AIBN) were dissolved in a LiTFSA/SL electrolyte and polymerized at 80 °C for 12 h (**Fig. S2**). The molar ratio of the monomer in the prepolymer solution was controlled at [LiTFSA]/[SL]/[monomer] = 1:3:*n* (*n* = 1, 1.5, and 2). The experimental details are described in the Electronic Supplementary Information (ESI†).

To investigate the effects of the polymer side chains on the solvation structure of Li^+ in the electrolytes, Raman spectra were collected for the polymer solutions with the composition of [LiTFSA]/[SL]/[monomer unit] = 1/3/*n*. Methacrylate monomer and an initiator (AIBN) was dissolved in the [LiTFSA]/[SL] = 1/3 solution and polymerized without a crosslinker to obtain a polymer solution. The Raman spectra for the polymer solutions (*n* = 1) and the [LiTFSA]/[SL] = 1/3 solution (without polymer) are shown in **Fig. 2**. The peak corresponding to the S–N–S stretching vibration of $TFSA^-$ was observed at 740–750 cm^{-1}. This peak is known to be sensitive to the complexation of TFSA with metal cations.[17–19] For $TFSA^-$ uncoordinated to metal cations, this peak is located at 739–742 cm^{-1}; in contrast, for $TFSA^-$ directly bound to Li^+ to form contact ion pairs (CIPs) and ionic aggregates (AGGs), the peak lies between 745 and 755 cm^{-1}. The S–N–S vibration peak of the [LiTFSA]/[SL] = 1/3 solution was observed at 744 cm^{-1}, suggesting that a certain amount of $TFSA^-$ was bound to Li^+. In the case of solution of polymerized PMA (PPMA), the TFSA peak appeared at a wavenumber comparable to that of the [LiTFSA]/[SL] = 1/3 solution; however, the peak shifted slightly toward a lower wavenumber when the PPMA content was further increased (*n* ≥ 1.5) (**Fig. S3**). This indicates that the carbonyl oxygen of PPMA was weakly coordinated to Li^+, and the CIPs and AGGs were slightly dissociated into ions. For the solution of polymerized TFPMA (PTFPMA), the TFSA peak position was independent of the polymer content and identical to that observed for the [LiTFSA]/[SL] = 1/3 solution (**Fig. S3**), suggesting that the polymer side chains did not coordinate or affect the solvation structure of Li^+. In sharp contrast, for the solution of polymerized DEGMA (PDEGMA), the TFSA peak clearly shifted toward a lower wavenumber in relation to that for the [LiTFSA]/[SL] = 1/3 solution, suggesting that this polymer enhanced the dissociations of CIPs and AGGs. It is well known that ether oxygen forms a complex with Li^+ owing to its strong electron-donating ability.[20] The donor numbers (DNs) of ether solvents (such as tetrahydrofuran and dimethoxyethane) are ca. 20 kcal mol^{-1}, while those of the TFSA anion and SL are 5.4 and 14.8 kcal mol^{-1}, respectively.[21,22] Therefore, the Li^+ ion as a Lewis acid prefers to coordinate to the ether side chain, which is the strongest Lewis base in the PDEGMA solution. In fact, the Raman peak for SO_2 vibration of SL in the PDEGMA solution appeared in the lower wavenumber compared with that in the [LiTFSA]/[SL] = 1/3 solution (**Fig. S4**), indicating that the fraction of free SL, which is uncoordinated to Li^+, was higher in the PDEGMA solution due to the complex formation of PDEGMA with Li^+. This also results in an enhanced dissociation of Li^+-$TFSA^-$.

Next, the effects of polymer side chains on the ion transport properties of gel electrolytes with crosslinked network structures were investigated. The ionic conductivity decreased with increasing polymer content of the gel electrolytes (**Fig. 3a** and **Fig. S5**). This is attributable to the decrease in the charge carrier number with increasing the polymer content as well as the obstruction of ion migration by the crosslinked polymer chains. The PPMA gel electrolyte exhibited a higher conductivity than the other gel electrolytes owing to its higher volume fraction of the liquid electrolyte (**Table S1**). The PDEGMA gel electrolyte exhibited a slightly higher conductivity than the PTFPMA gel electrolyte although its Li salt concentration was lower. The formation of complexes between Li^+ and ether moieties induces the dissociation of Li^+-$TFSA^-$ in PDEGMA (*vide supra*), while the partially fluorinated side chain does not interact with Li^+ in PTFPMA. The enhanced dissociation of Li^+-$TFSA^-$ in PDEGMA may explain the higher ionic conductivity of the gel electrolyte.

In addition to conductivity, the Li-ion transference number is an important characteristic of electrolytes. We evaluated the

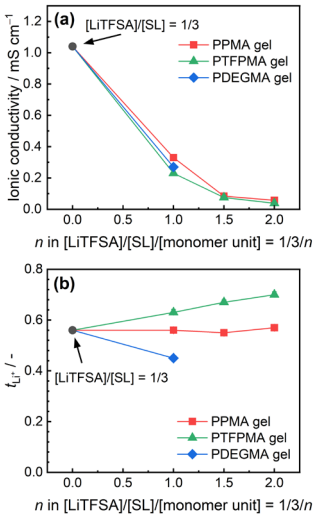

Fig. 3. (a) Ionic conductivity and (b) Li-ion transference numbers (t_{Li+}) of the [LiTFSA]/[SL] = 1/3 solution and the gel electrolytes [LiTFSA]/[SL]/[monomer unit] = 1/3/*n* at 30 °C.

Li-ion transference number (t_{Li+}) of the electrolytes under anion blocking conditions using Li/Li symmetric cells (**Fig. S6–S8**).[23,24] The PPMA gel electrolytes exhibited t_{Li+} values comparable to that of the parent electrolyte solution ([LiTFSA]/[SL] = 1/3), almost independent of the PPMA content (**Fig. 3b**). This is attributed to Li^+-hopping conduction occurring in SL-based HCEs used in this study, resulting in a higher mobility of Li^+ than that of the anions.[20,21,25] Thus, the SL-based HCEs exhibit relatively high t_{Li+} values (>0.5) than conventional carbonate-based electrolytes containing approximately 1 M Li salts ($t_{Li+} \approx 0.3$).[5,8] In the PPMA network, the interactions between the polymer side chains and ions are weak (*vide supra*), and the ion conduction mechanism in the parent electrolyte is preserved after PPMA gel formation. In fact, pulsed-field gradient (PFG) nuclear magnetic resonance (NMR) spectroscopy revealed that the diffusivity of Li^+ (D_{Li^+}) was higher than that of $TFSA^-$ (D_{TFSA^-}) in both the parent and PPMA gel electrolytes (**Table S2** and **Fig. S9**). In contrast, the t_{Li+} of the PDEGMA gel electrolyte (n = 1) (0.45) was lower than that of the parent electrolyte (0.56). The ethylene glycol group of PDEGMA formed a complex with Li^+ (*vide supra*), and the polymer chains could not migrate macroscopically in the crosslinked gel. Consequently, the side chains in PDEGMA trapped Li^+ ions, thereby lowering the mobility of Li^+ relative to that of $TFSA^-$ and decreasing the t_{Li+} value of the gel electrolyte. Surprisingly, the PTFPMA gel electrolytes exhibited larger t_{Li+} values than the parent electrolyte. The t_{Li+} value increased with the polymer content and reached 0.70 for [LiTFSA]/[SL]/[TFPMA] = 1/3/2. The diffusivity ratio of Li^+ relative to the anion (D_{Li^+}/D_{TFSA^-}) in the PTFPMA gel electrolyte was higher than that in the parent electrolyte (**Table S2** and **Fig. S9**), indicating that the mobility of $TFSA^-$ was lowered relative to that of Li^+ in the gel electrolyte. As mentioned previously, the side chain of PTFPMA is not coordinated with Li^+; therefore, the PTFPMA network retains the solvation structure of the parent electrolyte. Our hypothesis is that the partially fluorinated side chain of PTFPMA interacts with $TFSA^-$. To understand the electrophilicity of the side chains, electrostatic potential (ESP) maps of monomers were calculated. For the TFPMA monomer with a partially fluorinated alkyl side chain, a highly acidic proton surrounded by electron-withdrawing fluorine atoms was found at the end of the side chain (**Fig. S10**). DFT calculations show that the interaction of $TFSA^-$ anion with TFPMA monomer is much stronger than that with PMA monomer, suggesting that the positively charged acidic protons of the PTFPMA side chains interact electrostatically with the $TFSA^-$ anions (**Fig. S11**). Therefore, the PTFPMA polymer traps anions, resulting in a higher t_{Li+} of the corresponding gel electrolytes.

Furthermore, the electrochemical windows of the PPMA and PTFPMA gel electrolytes (n = 1) were investigated. In the linear sweep voltammograms, both gel electrolytes exhibited oxidative stability comparable to that of the parent electrolyte solution (**Fig. S12**). The SL solvent itself is oxidatively stable, but its reductive stability is poor, and SL decomposition occurs on the Li metal.[25,26] However, the reductive decomposition of SL can be suppressed by increasing the LiTFSA concentration. The suppression of reductive decomposition can be explained by the TFSA-derived passivation layer on the Li metal and the low concentration of the SL solvent in the electrolyte.[25,27] In fact, reversible Li deposition and dissolution were observed at the interface between a Cu electrode and the gel electrolytes (**Fig. S13**).

Finally, the rate capabilities of the PPMA and PTFPMA gel electrolytes in 4 V class batteries were evaluated to investigate the effects of ion transport properties on battery performance (**Fig. S14**). For the cells with a structure of [Li | gel electrolyte membrane (500 μm thick) | $LiCoO_2$], discharge curves were recorded at various current densities (**Fig. 4** and **Fig. S15**). At a lower current density (0.15 mA cm^{-2}), both types of cells exhibited a discharge capacity of 140 mAh g^{-1} based on the mass of $LiCoO_2$. This is close to the theoretical capacity (137 mAh g^{-1}) for the electrochemical reaction of $LiCoO_2/Li_{0.5}CoO_2$ in the voltage range of 3.0–4.2 V. The discharge capacities decreased with increasing current density because of the limitation of Li^+ diffusion in the gel electrolytes.[28,29] The discharge capacity of the PPMA cell decreased gradually when increasing the current density to >0.45 mA cm^{-2}. In contrast, the discharge capacity of the PTFPMA cell remained nearly constant at current densities lower than 0.75 mA cm^{-2} and decreased gradually at above 1.05 mA cm^{-2}. The capacity retentions at 1.50 mA cm^{-2} (1C) relative to the theoretical capacity of $LiCoO_2$ were 40 % and 80 % for the PPMA and PTFPMA cells, respectively. Despite the lower ionic conductivity of PTFPMA than that of PPMA, the PTFPMA cell showed a higher rate capability. This can be explained by the mitigation of concentration polarization in the PTFPMA cell owing to the higher t_{Li+} of the PTFPMA gel electrolyte. When a cell discharges at a high current density, the Li salt concentration increases and decreases near the anode and cathode, respectively, and a concentration gradient is formed across the gel electrolyte, causing concentration polarization. Concentration polarization lowers the discharge voltage of the cell, and the cutoff voltage (3.0 V) is reached before the full cell

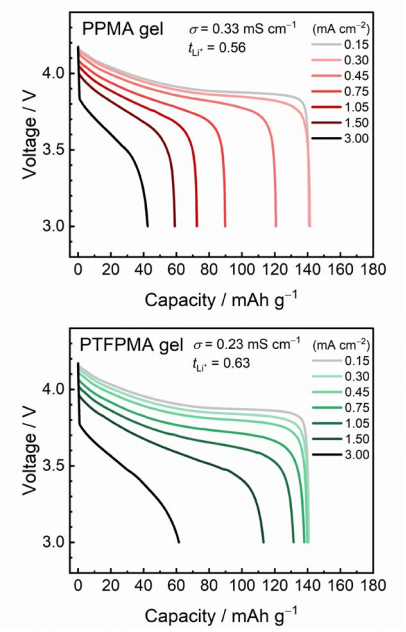

Fig. 4. Discharge curves of Li/$LiCoO_2$ cells with gel electrolytes [LiTFSA]/[SL]/[monomer unit] = 1/3/1 at 30 °C.

capacity is achieved. In fact, the slopes of the discharge curves of cells become steeper with increasing current density, indicating that concentration polarization becomes larger with increasing current density. At a high t_{Li+} value, the development of concentration gradient in the electrolyte layer is effectively suppressed, thereby decreasing the concentration overpotential of the cell.[28,30] Consequently, both the ionic conductivity and t_{Li+} of the electrolyte significantly affect the rate capability of LIBs. In this work, the gel electrolyte layer was thicker (500 μm) than commercial separators for LIBs (<20 μm). To achieve high rate capability in a LIB, the use of a thinner electrolyte layer is effective because it can increase the diffusion-limiting current density.

In summary, we investigated the effects of different polymer side chains on the ion transport properties and battery performance of the gel electrolytes containing thermally stable SL-based HCEs. We found that the t_{Li+} value of the gel electrolytes depends on the functional group of the side chain. The PPMA network with a simple alkyl side chain interacted very weakly with Li^+; thus, the t_{Li+} of the PPMA gel electrolyte was almost identical to that of the parent SL-based electrolyte. In the case of PDEGMA gel, the ether side chains of PDEGMA were coordinated to Li^+ ions, and the mobility of Li^+ was reduced by the PDEGMA matrix, resulting in a lower t_{Li+} value. Notably, PTFPMA with partially fluorinated side chains interacted with $TFSA^-$ anions but not with Li^+, and the mobility of the anion is reduced, resulting in a higher t_{Li+} than that of the parent electrolyte. The higher t_{Li+} of the PTFPMA gel electrolyte effectively suppressed concentration polarization in the $Li/LiCoO_2$ cell. Although the ionic conductivity of the electrolytes decreased after gelation, the t_{Li+} value can be increased by using a polymer network with functional groups that interact with anions but not with Li^+. This study provides insights into the effects of side chains in the polymer network on the ion transport properties of gel electrolytes, promoting the design of gel electrolytes with high Li-ion transport abilities for LIBs and Li metal batteries.

Acknowledgements

This study was partially supported by JSPS KAKENHI (Grant Nos. JP21H04697, JP22H00340, and JP23K17370) from the Japan Society for the Promotion of Science (JSPS) and by GteX Program Japan (Grant No. JPMJGX23S0) of the Japan Science and Technology Agency (JST).

Conflicts of interest

There are no conflicts to declare.

Data availability

The data supporting this article have been included as part of the ESI.

Notes and references

1 K. Xu and C. A. Angell, *J. Electrochem. Soc.*, 2002, **149**, A920–A926.
2 A. Abouimrane, I. Belharouak, and K. Amine, *Electrochem. Commun.*, 2009, **11**, 1073–1076.
3 Y. Yamada and A. Yamada, *J. Electrochem. Soc.*, 2015, **162**, A2406–A2423.
4 Y. Yamada, J. Wang, S. Ko, E. Watanabe and A. Yamada, *Nat. Energy*, 2019, **4**, 269–280.
5 Y. Ugata, K. Shigenobu, R. Tatara, K. Ueno, M. Watanabe and K. Dokko, *Phys. Chem. Chem. Phys.*, 2021, **23**, 21419–21436.
6 K. Dokko, D. Watanabe, Y. Ugata, M. L. Thomas, S. Tsuzuki, W. Shinoda, K. Hashimoto, K. Ueno, Y. Umebayashi and M. Watanabe, *J. Phys. Chem. B*, 2018, **122**, 10736–10745.
7 A. Nakanishi, K. Ueno, D. Watanabe, Y. Ugata, Y. Matsumae, J. Liu, M. L. Thomas, K. Dokko and M. Watanabe, *J. Phys. Chem. C*, 2019, **123**, 14229–14238.
8 Y. Ugata, Y. Chen, S. Sasagawa, K. Ueno, M. Watanabe, H. Mita, J. Shimura, M. Nagamine and K. Dokko, *J. Phys. Chem. C*, 2022, **126**, 10024–10034.
9 W. H. Meyer, *Adv. Mater.*, 1998, **10**, 439−448.
10 L. Long, S. Wang, M. Xiao, and Y. Meng, *J. Mater. Chem. A*, 2016, **4**, 10038−10069.
11 F. Wan, K. Hu, R. Liu, S. Zhang, S. Li, Y. Lei, D. Yang, C. Wang, Y. Xia and W. Chen, *Chem. Commun.*, 2024, **60**, 7220–7223.
12 Z. Wang, L. Shen, S. Deng, P. Cui and X. Yao, *Adv. Mater.* 2021, **33**, 2100353.
13 Z. Zhang, Z. Cheng, F. Qiu, Y. Jiang, M. Jia, X. Yan and X. Zhang, *Chem. Commun.*, 2024, **60**, 6276–6279.
14 Z. Xu, Z. Liu, Z. Gu, X. Zhao, D. Guo and X. Yao, *ACS Appl. Mater. Interfaces*, 2023, **15**, 7014–7022.
15 K. Hashimoto, R. Tatara, K. Ueno, K. Dokko and M. Watanabe, *J. Electrochem. Soc.*, 2021, **168**, 090538.
16 N. Tasaki, Y. Ugata, K. Hashimoto, H. Kokubo, K. Ueno, M. Watanabe and K. Dokko, *Phys. Chem. Chem. Phys.*, 2023, **25**, 17793–17797.
17 Y. Umebayashi, T. Mitsugi, S. Fukuda, T. Fujimori, K. Fujii, R. Kanzaki, M. Takeuchi and S. I. Ishiguro, *J. Phys. Chem. B*, 2007, **111**, 13028–13032.
18 D. M. Seo, P. D. Boyle, R. D. Sommer, J. S. Daubert, O. Borodin and W. A. Henderson, *J. Phys. Chem. B*, 2014, **118**, 13601–13608.
19 W. A. Henderson, M. L. Helm, D. M. Seo, P. C. Trulove, H. C. De Long and O. Borodin, *J. Electrochem. Soc.*, 2022, **169**, 060515.
20 Z. Xue, D. He and X. Xie, *J. Mater. Chem. A*, 2015, **3**, 19218–19253.
21 W. Linert, A. Camard, M. Armand and C. Michot, *Coord. Chem. Rev.*, 2002, **226**, 137–141.
22 K. Izutsu, Electrochemistry in Nonaqueous Solutions, Wiley-VCH Verlag GmbH & Co. KGaA, Weinheim, Germany, 2nd edn., 2009.
23 J. Evans, C. Vincent and P. Bruce, *Polymer*, 1987, **28**, 2324–2328.
24 M. Galluzzo, J. Maslyn, D. Shah and N. Balsara, *J. Chem. Phys.*, 2019, **151**, 020901.
25 Y. Ugata, R. Tatara, T. Mandai, K. Ueno, M. Watanabe and K. Dokko, *ACS Appl. Energy Mater.*, 2021, **4**, 1851–1859.
26 T. Kaneko and K. Sodeyama, *Chem. Phys. Lett.*, 2021, **762**, 138199.
27 Y. Yamada, K. Furukawa, K. Sodeyama, K. Kikuchi, M. Yaegashi, Y. Tateyama and A. Yamada, *J. Am. Chem. Soc.*, 2014, **136**, 5039–5046.
28 M. Doyle, T. F. Fuller and J. Newman, *Electrochem. Acta*, 1994, **39**, 2073–2081.
29 K. Yoshida, M. Tsuchiya, N. Tachikawa, K. Dokko and M. Watanabe, *J. Electrochem. Soc.*, 2012, **159**, A1005–A1012.
30 K. M. Diederichsen, E. J. McShane and B. D. McCloskey, *ACS Energy Lett.*, 2017, **2**, 2563–2575.

Data availability

The data supporting this article have been included as part of the ESI.